Graduate School of Oceanography Faculty Publications

Graduate School of Oceanography

Near-Bottom Circulation and Dispersion of Sediment Containing Alexandrium fundyense Cysts in the Gulf of Maine During 2010–2011

Alfredo L. Aretxabaleta

Bradford Butman

Richard P. Signell

P. Soupy Dalyander

Christopher R. Sherwood

See next page for additional authors

Citation/Publisher Attribution

Near-Bottom Circulation and Dispersion of Sediment Containing Alexandrium fundyense Cysts in the Gulf of Maine During 2010–2011

Creative Commons License

Authors

Alfredo L. Aretxabaleta, Bradford Butman, Richard P. Signell, P. Soupy Dalyander, Christopher R. Sherwood, Vitalii A. Sheremet, and Dennis J. McGillicuddy Jr.

Near-bottom circulation and dispersion of sediment containing *Alexandrium fundyense* cysts in the Gulf of Maine during 2010–2011

Alfredo L. Aretxabaleta [a,b,*], Bradford Butman [a], Richard P. Signell [a], P. Soupy Dalyander [a], Christopher R. Sherwood [a], Vitalii A. Sheremet [c], Dennis J. McGillicuddy Jr.[d]

[a] U.S. Geological Survey, Woods Hole, MA, USA
[b] Integrated Statistics, Woods Hole, MA, USA
[c] University of Rhode Island, Narragansett, RI, USA
[d] Woods Hole Oceanographic Institution, Woods Hole, MA, USA

ARTICLE INFO

ABSTRACT

The life cycle of *Alexandrium fundyense* in the Gulf of Maine includes a dormant cyst stage that spends the winter predominantly in the bottom sediment. Wave-current bottom stress caused by storms and tides induces resuspension of cyst-containing sediment during winter and spring. Resuspended sediment could be transported by water flow to different locations in the Gulf and the redistribution of sediment containing *A. fundyense* cysts could alter the spatial and temporal manifestation of its spring bloom. The present study evaluates model near-bottom flow during storms, when sediment resuspension and redistribution are most likely to occur, between October and May when *A. fundyense* cells are predominantly in cyst form. Simulated water column sediment (mud) concentrations from representative locations of the Gulf are used to initialize particle tracking simulations for the period October 2010–May 2011. Particles are tracked in full three-dimensional model solutions including a sinking velocity characteristic of cyst and aggregated mud settling (0.1 mm s^{-1}). Although most of the material was redeposited near the source areas, small percentages of total resuspended sediment from some locations in the western ($\sim$4%) and eastern (2%) Maine shelf and the Bay of Fundy (1%) traveled distances longer than 100 km before resettling. The redistribution changed seasonally and was sensitive to the prescribed sinking rate. Estimates of the amount of cysts redistributed with the sediment were small compared to the inventory of cysts in the upper few centimeters of sediment but could potentially have more relevance immediately after deposition.

© 2013 Elsevier Ltd. All rights reserved.

1. Introduction

The Gulf of Maine (GoM), located off the U.S. northeast coast, exhibits a generally cyclonic mean circulation (Bigelow, 1927; Brooks and Townsend, 1989). The main circulation feature is the Maine Coastal Current (MCC) that flows southwestward from the Bay of Fundy to Massachusetts Bay, with a bifurcation point offshore of Penobscot Bay where part of the current flows offshore. Flow variability characterization has been aided by modeling results (Brooks, 1994; Lynch et al., 1997; Xue et al., 2000; Pettigrew et al., 2005) and more recently observations (Manning et al., 2009; Li et al., 2014). The circulation in the adjacent Bay of Fundy (BoF) is dominated by strong tides (Garrett, 1972; Greenberg, 1983) and the presence of a persistent counter-clockwise gyre at its entrance (Aretxabaleta et al., 2008, 2009). The main focus of the circulation studies in the GoM has been on the surface or depth-averaged flow. The understanding of near-bottom flow includes information obtained from a few seabed drifter trajectories in the eastern GoM (Lauzier, 1967), a pair of moorings over the central Maine shelf (Vermersch et al., 1979; Brown and Beardsley, 1978), and monthly average velocity from two stations over the central and eastern Maine shelf (Pettigrew et al., 2005; Churchill et al., 2005). The reported direct velocity measurements were obtained between 20 and 30 m off the seafloor.

The circulation of the GoM is a significant factor in the dynamics of *Alexandrium fundyense* blooms (McGillicuddy et al., 2005). *A. fundyense* is a toxic dinoflagelate that causes extensive shellfish toxicity during spring and summer when blooms occur. The life cycle of *A. fundyense* includes a dormant cyst state (Anderson and Wall, 1978; Anderson et al., 2005a). *A. fundyense* cells germinate from resting cysts in early spring and summer of each year and rapidly divide, regularly resulting in Harmful Algal Blooms (Anderson et al., 2005b). When the bloom subsides, the *A.*

---

fundyense cells form dormant cysts that deposit in the bottom sediment. Cysts have also been observed in the benthic nepheloid layer (Kirn et al., 2005; Pilskaln et al., 2014). High concentrations of cysts in the sediment are generally encountered in two regions: the entrance to the Bay of Fundy (Martin et al., 2014) and the Maine shelf offshore of Penobscot Bay (Anderson et al., 2014).

The potential effect of sediment resuspension on the population of *A. fundyense* cysts has been investigated by (Butman et al., 2014). From fall until spring, sediment is episodically resuspended by enhanced bottom stress caused by tidal currents and oscillatory wave-induced currents with varying importance depending on location (wave stress being largest in shallow water and tidal stress increasing from west to east). Their results suggest that around 1 mm of sediment (and associated cysts) can be resuspended by strong storms during winter and spring. The resuspended sediment could then be transported laterally thus potentially modifying the spatial cyst distribution. Additionally, cysts resuspended during spring, when they are viable, would also be subject to increased light favorable for germination and growth.

The behavior of water-borne particles in the Gulf of Maine has been studied through observational (Manning et al., 2009) and modeling (Hannah et al., 1998; Xue et al., 2008; Li et al., 2014) approaches. Manning et al. (2009) analyzed drifter observations to produce estimates of transit time across different isobaths. The dispersion of various organisms (the copepod Calanus finmarchicus, Hannah et al. (1998); lobster larvae, Xue et al. (2008); and *A. fundyense* blooms Li et al. (2014)) has been simulated using numerical particle tracking.

The concept of connectivity has been applied predominantly to ecological studies in which Lagrangian particle tracking has been used to characterize larval dispersal and to define open versus closed populations (Cowen et al., 2006). An open population receives larvae from other locations, while a closed population receives larvae primarily from local spawning activity (Cowen et al., 2006; Mora and Sale, 2002; Cowen et al., 2007; Edwards et al., 2007). One of the benefits of using individual-based approaches is the possibility of incorporating behavior to the description of connectivity (Cowen et al., 2007).

Li et al., 2014, studied connectivity in the surface with the purpose of relating *A. fundyense* sources with their most likely destinations after the bloom was initiated. Their results suggest that surface connectivity exhibited significant interannual variability and was dominated by the transport of particles by the MCC and the retention associated with the Bay of Fundy gyre. The focus of Li et al., 2014, and other studies was on surface or near-surface dynamics, but connectivity is likely different for bottom-dominated processes.

Butman et al., 2014, calculated sediment concentration in the water column at seven stations covering representative sedimentary and hydrodynamic areas of the Gulf. They used erodibility profiles that matched measured characteristics and wave-current bottom stress to estimate erosion in the bed and suspended sediment in the water. In order to examine sediment transport pathways, the present study uses velocity for the Gulf of Maine from archived Finite Volume Coastal Ocean Model (FVCOM: Chen et al., 2003) simulations. Model results are compared to a set of recently developed tilt meter current observations and ADCP velocities from a regional observation system. Even though the largest sediment concentration is found near-bottom, suspended concentrations are found throughout the entire water column. Thus, the full three-dimensional FVCOM flow is used to track sediment in the water column to determine the likely deposition location of resuspended material. The connectivities between the different locations for both sediment and cyst concentrations are characterized under different seasonal and settling velocity scenarios.
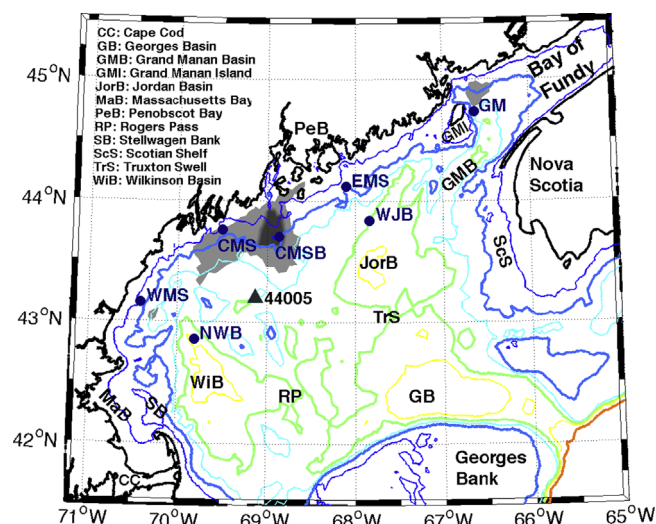

Fig. 1. Model domain (FVCOM) for the Gulf of Maine and Bay of Fundy. The locations of the seven stations where sediment resuspension data were available (Butman et al., 2014) are shown (blue): WMS, Western Maine Shelf; NWB, Northern Wilkinson Basin; CMS, Central Maine Shelf; CMSB, Central Maine Seed Bed; WJB, Western Jordan Basin; EMS, Eastern Maine Shelf; and GM, Grand Manan. The position of NDBC Buoy 44005 is also marked. The location of the two cyst concentration maxima during 2011 (around CMSB and GM) are indicated with the 500 (light gray) and 1000 (dark gray) cyst cm^{-3} filled contours. The 50 (blue), 100 (thick blue), 150 (light blue), 200 (thick orange), 250 (yellow), and 500 (thick red) m isobaths are shown.

2. Methods

2.1. Model

Archived modeled currents were obtained from the Northeast Coastal Ocean Forecast System (NECOFS) which uses the FVCOM model. FVCOM is a prognostic, unstructured grid, finite-volume, primitive equation circulation model. The NECOFS implementation includes the entire Gulf of Maine and Bay of Fundy (Fig. 1) with open ocean boundaries along the New Jersey and Scotian shelves. Hourly values were downloaded from the hindcast archive (http://www.smast.umassd.edu:8080/thredds/dodsC/fvcom/archives/necofs gom3.html).

The NECOFS implementation has 40 layers in the vertical and the height of the bottom layer above the seafloor ranged from greater than 2.5 m in the deep basins to less than 0.5 m over the shelf.

Our procedure took advantage of the availability of the entire model solution archived on a THREDDS server (http://www.unidata.ucar.edu/projects/THREDDS/tech/TDS.html, Signell, 2010). Instead of needing a locally run simulation (computationally expensive for a large domain for long periods) or having to download the full model solution (large dataset, ~1 TB per year), we accessed only the velocities needed in the vicinity of the previous tracked particle position to produce the tracking for each particle location and time. This strategy took advantage of reliable connections to remote servers to avoid the duplication of large datasets.

The FVCOM model velocities were used in (Butman et al., 2014) in combination with bottom orbital velocities generated using the Simulating Waves Nearshore (SWAN) model (Holthuijsen et al., 1993) to create time-series of wave-current bottom stress for the period October 1, 2010 - May 31, 2011. FVCOM velocities also provided boundary conditions for one-dimensional (vertical) resuspension simulations at seven locations in the GoM.

Table 1
Station identifier, location, water depth, sediment texture and average mass of suspended mud. Percentage sand and mud (combined silt and clay) from cores collected during 2011 (OC477) with percentages for 2010 (EN486) in italics. The remaining percentage corresponds to gravel. Note the increase in sand fraction at stations WMS and EMS between 2010 and 2011. Suspended mud (combined 8 μm and 2 μm sediment classes) is the average concentration estimated by the model resuspension experiments integrated in the vertical.

Name	Location	Depth (m)	% sand	% mud	Suspended mud (kg m^{-2})
WMS	Western Maine shelf	71	79.1 (30.9)	17.2 (69.1)	0.0325
NWB	Northern Wilkinson Basin	265	0.2 (0.3)	99.8 (99.7)	0.0
CMS	Central Maine shelf	95	5.3 (5.9)	94.7 (94.1)	0.0399
CMSB	Central Maine seed bed	103	1.3 (3.7)	98.7 (96.3)	0.0177
WJB	Western Jordan Basin	201	11.0 (7.8)	88.4 (92.2)	0.0001
EMS	Eastern Maine shelf	88	30.5 (5.0)	63.5 (95.0)	0.2210
GM	Grand Manan Island	122	10.8 (7.3)	89.1 (92.7)	0.1020

2.2. Sediment resuspension data

(Butman et al., 2014) used the Regional Ocean Modeling System (ROMS) in combination with the Community Sediment Transport Modeling System (CSTMS, Warner et al., 2008) to calculate sediment resuspension and water column concentrations during winter (October 2010–March 2011) and spring (April–May 2011). The CSTMS implementation considered the cohesive behavior of the sediment bed (following Sanford and Maa, 2001 and Sanford, 2008) based on erodibility profiles modeled after observed erodibility curves in sediment cores measured with a University of Maryland Gust Erosion Microcosm System (UGEMS, Gust and Mueller, 1997).

Numerical resuspension simulations were conducted by (Butman et al., 2014) at seven locations where sediment cores were collected during a cruise in October 2011 (R/V Oceanus cruise 477, OC477). These sites have different depth, sediment, wave, and hydrodynamical conditions (Fig. 1, Table 1): western Maine shelf (WMS), northern Wilkinson Basin (NWB), central Maine shelf (CMS), central Maine seed bed (CMSB), eastern Maine shelf (EMS), western Jordan Basin (WJB), and Grand Manan (GM). One-dimensional (vertical) implementations of ROMS were run for each of the seven locations with 50 vertical layers. The model internally calculated bottom roughness lengths based on sediment grain roughness, sediment transport, and bedform roughness. The velocity boundary conditions were obtained from the archived FVCOM model run. Bottom wave orbital velocity for each location was approximated from SWAN simulations that provided a significant wave height and a dominant wave period. The resuspension calculations included three sediment classes that represented the fractional distribution observed in the sediment cores: one sand class (125 μm), one silt class (8 μm) and one clay class (2 μm). The settling velocity of the sand particles was calculated to be 8 mm s^{-1} using the Dietrich (1982) formulation. The settling speed of both mud classes (silt and clay) was assigned to be 0.1 mm s^{-1} as mud was expected to be present primarily as flocculated particles.

The settling velocities of aggregated particles at minimum concentrations in Winterwerp (2002) ranged from 0.05 to 0.3 mm s^{-1} with the median being around 0.1 mm s^{-1}. The value of 0.1 mm s^{-1} was also consistent with described estimates of aggregated mud (flocculated particles) for other shelf environments (Hill et al., 2000; Bever et al., 2009). The mud settling speed matched the observed settling velocity of *A. fundyense* cysts (Anderson et al., 1985). Erodibility of the cohesive bed in the model was implemented as a property of the bed which depended on a bulk critical shear stress that increased with depth in the sediment. The UGEMS measurements showed that erosion began at about 0.05 Pa but the rate varied with sediment depth depending on location. Sediment at sandy stations (WMS, EMS) was less erodible than at muddy locations. The wave-current bottom stress (Fig. 2) was caused primarily by tidal and, in shallower water, wave-driven orbital velocities. Tidal currents were largest in the Bay of Fundy, where wave-induced stress was minimal because of limited fetch. Tidal currents decreased westward to a minimum in the western Maine shelf, while wave bottom stress was larger in shallower areas with diminished effects below 100 m.

The model resuspension time series (Fig. 2) showed that the peaks in suspended sediment were generally a result of wave stress associated with storm events in water depths of 100 m or less (WMS, CMS, CMSB, and EMS). In deeper stations (NWB and WJB) and in the BoF (GM) wave stress was reduced and did not result in resuspension. Stress caused by tidal current added a variable background stress, mostly in semidiurnal frequencies, that increased to the east and was largest at GM, where it was the main cause of sustained resuspension. Resuspended mud was more abundant than sand in the water column because the majority of the bed consisted of fine sediment (Table 1) and because of the slower settling speed of mud. The average suspended mud concentration (Table 1) was largest at EMS (0.22 kg m^{-2}) and GM (0.1 kg m^{-2}). The western and central Maine shelf stations also exhibited resuspension but their average magnitudes were substantially smaller. A complete description of the observations and model results can be found in (Butman et al., 2014).

2.3. Tracking methodology

In the present study, resuspended sediment was represented as particles in the three-dimensional FVCOM current field and were tracked to provide an estimate of the redistribution of sediments. Particles were released according to the sediment concentration calculated by the one-dimensional resuspension simulations, and then transported by the velocity field. Particles were not strictly passive, however, as they also sank at the specified settling speed associated with each sediment class. When particles crossed the bottom boundary of the domain because of their settling velocity, they were assumed to have deposited and were no longer tracked. The Lagrangian simulations provided an estimate of the distance traveled for each resuspension event. The Lagrangian simulations did not include the possibility of the sediment being resuspended after the first deposition event and thus they represent conservative estimates for total transport.

The simulated resuspension results were sampled every 3 h to determine the vertical distribution of sediment in the water column and an ensemble of particles proportional to modeled concentration was released and tracked for the duration of the experiment (October–May) for each of the sediment classes. Particles were not released when there was no sediment at a specific vertical layer, resulting in a variable total number of tracked particles for each station. The maximum number of particles tracked was 45 million at station EMS. Less resuspension at the deep basin stations resulted in fewer particles been tracked. At WJB, only 200,000 particles were tracked and NWB required no particles as the model estimated no resuspension there (Fig. 2).
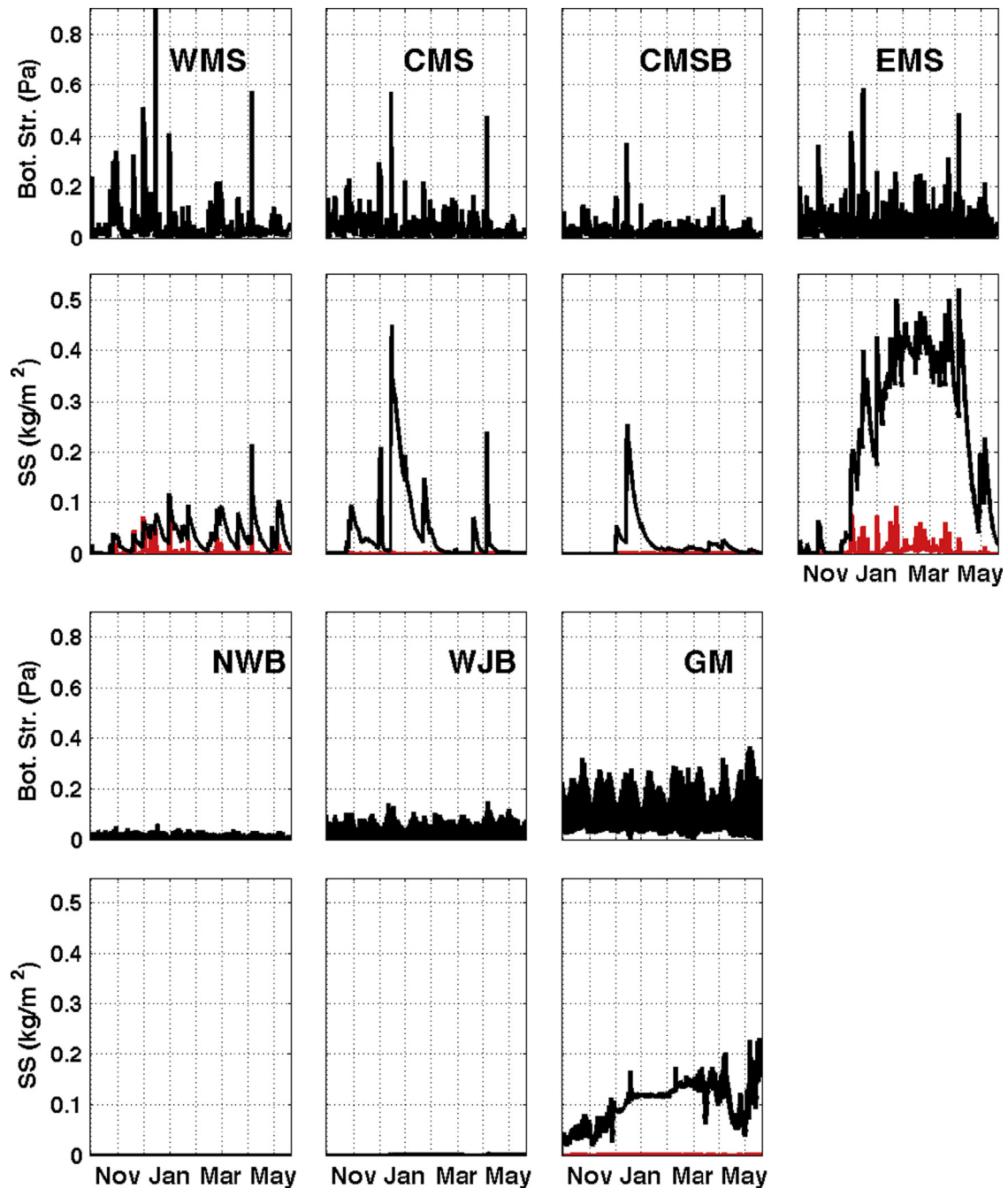
Fig. 2. Results of the resuspension simulation at WMS, CMS, CMSB, EMS, NWB, WJB, and GM for the period October 1, 2010 May 31, 2011. For each station, the top row shows the time series of wave-current bottom stress (in Pa); the second row shows the integrated suspended sediment in the water column (SS) for sand (125 μm, red) and mud (2 and 8 μm together, black).

The numerical particle trajectories were calculated with an offline particle tracking model (DROGUE3D, Blanton, 1993) using the archived simulated FVCOM currents. The Lagrangian tracking included a 4th-order Runge–Kutta scheme for advection. A reflective boundary condition was applied to prevent particles from exiting the horizontal edge of the domain or escaping through the bottom or surface. Particles that hit the land boundary were reflected back, so particles were kept within the model domain, except when they deposited on the bottom via vertical settling velocity. The particles' turbulent behavior in the vertical was not included in the particle tracking as vertical turbulent eddy viscosity was not provided with the archived simulations. Enhanced vertical diffusivity near the bottom would maintain particles in suspension for longer periods of time, thereby increasing lateral transport. This factor also suggests that the calculated redistributions represent conservative estimates.

The settling velocity of the particles was crucial to estimate the redistribution of sediment containing *A. fundyense* cysts. The measured settling velocity of *A. fundyense* cysts is on the order of 0.1 mm s^{-1} (0.08–0.13 mm s^{-1}, Anderson et al., 1985) which is consistent with the sinking rate of aggregated mud in shelf environments (Hill et al., 2000; Winterwerp, 2002; Bever et al., 2009). The value of 0.1 mm s^{-1} was chosen as the default particle settling speed (consistent with the sinking speed from Butman et al., 2014) and it was used in all simulations unless indicated otherwise. To study the sensitivity to settling speed, additional values were used to provide a range of redistributions. *A. fundyense* cysts have an ellipsoidal shape with dimensions 47×30 μm

(Anderson and Wall, 1978, ranging from 40 to 47 and 24 to 30 µm, Anderson et al., 1985). The settling velocity of a sediment particle of equivalent size using the Dietrich (1982) formulation would be around 1 mm s^{-1} (0.6–1.3 mm s^{-1} range). Additionally, the settling velocity of a single (not aggregated) particle of mud (taken to be 8 µm in size) provided by the Dietrich formulation was 0.04 mm s^{-1}. The selected fast and slow estimates were chosen to simulate a reasonable envelope of redistribution.

3. Results

3.1. Flow characterization

3.1.1. Bottom velocity observations

While the Maine Coastal Current (Brooks, 1994; Lynch et al., 1997; Xue et al., 2000; Pettigrew et al., 2005) is the dominant flow in the surface and sub-surface in the Gulf of Maine, the near-bottom circulation is characterized by temporally varying subregional flows influenced by bathymetric features. Observed velocities in the lower part of the water column were sparse during the period of interest (October 2010 – May 2011). Time series covering the entire period were available from ADCP measurements collected at six locations as a part of the Gulf of Maine Ocean Observing System (now part of the

North-eastern Regional Association of Coastal and Ocean Observation Systems, NERACOOS, http://www.neracoos.org, Pettigrew et al., 2011). The lowermost ADCP bin from each NERACOOS location ranged 6–20 m off the bottom, and sometimes did not represent flows in the bottom boundary layer, which were of particular interest to the present application.

A data set of near-bottom current observations was obtained from the SeaHorse Tilt Current meters developed by Sheremet as a part of eMOLT project (http://www.nefsc.noaa.gov/epd/ocean/MainPage/tilt/shtcm.html). The instrument uses a triple axis accelerometer measuring the flow drag induced tilt of a tethered buoyant PVC pipe. The current meters were attached to lobster traps, deployed at locations of opportunity as a part of the eMOLT project (Manning and Pelletier, 2009), and measured currents at around 0.8 m above bottom. During the study period, the length of deployment of the tilt current meter ranged from two weeks to two months but their spatial coverage provided a valuable complement to the NERACOOS ADCP data (Fig. 3A). The currents measured with the tilt meters exhibited some deficiencies during 2010 caused by the lobster traps changing direction during hauling or sporadically during times of intense currents and waves. To avoid the introduction of directional issues, only the speed of the currents was used in this study as a more robust variable. The 2010 instruments represented an early prototype design that evolved
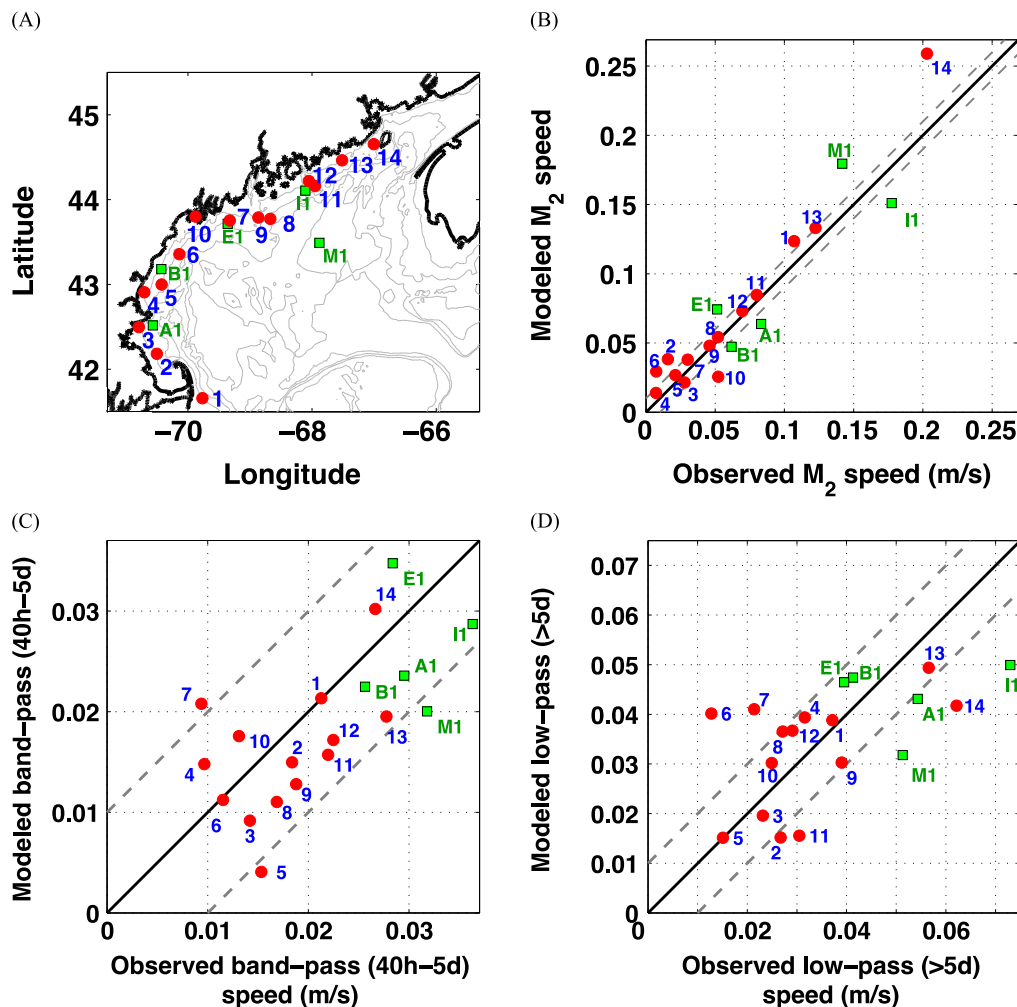
Fig. 3. Model-data comparison with red dots (blue numbers) indicating eMOLT, and green squares showing NERACOOS ADCPs. (A) Location of the stations. (B) Comparison between the observed (x-axis) and modeled (y-axis) M_2 tidal constituent speed from a harmonic analysis using t_tide (Pawlowicz et al., 2002). (C) Comparison between the observed and modeled band-pass filtered RMS speed in the band between 40 h and 5 days. (D) Comparison between the observed and modeled low-pass filtered RMS speed with a 5-day cutoff period. The 1 − 1 line (solid black) and a 0.01 m s^{-1} error envelope (dashed gray lines) are included in the speed comparisons. Note the speed magnitude scale change between panels.

since their first deployment on traps in 2008. The most recent 2013 model is more accurate and has a digital compass incorporated to derive the absolute velocity direction.

The observed bottom flow was mainly tidally driven, with tides explaining between 60 and 85% of the current variance, with increasing importance toward the northeast. Observed near-bottom tidal currents (estimated using the t_tide (Pawlowicz et al., 2002) harmonic analysis), defined by the M2 tidal speed, were weakest at the southwestern stations (along the Massachusetts, New Hampshire and western Maine coast), and strongest in the vicinity of the Bay of Fundy (Fig. 3B). The tidal currents from the lowermost NERACOOS ADCP bin were larger than near-bottom currents measured by nearby eMOLT tilt meters. M2 tidal speed at E1, 6 m off the bottom, was 0.05 m s^{-1}, while being 0.03 m s^{-1} near the bottom at nearby eMOLT 7. At NERACOOS station I 1, 10 m off the bottom, the tidal speed was 0.18 m s^{-1} and at eMOLT 11, 0.08 m s^{-1}. Thus, the lowermost ADCP measurements might overestimate the near-bottom velocity due to the shear in the bottom boundary layer.

To investigate the relative importance of flow at different frequencies, the sub-tidal near-bottom velocity was filtered using two complementary bands: a band-pass filter, with cutoff frequencies equivalent to 40 h and 5 days, that isolated wind-band flows (associated with the passage of storms, Fig. 3C); and a low-pass filter, with a 5-day cutoff frequency, that represented longer period flow fluctuations (Fig. 3D). The observed wind-band near-bottom speed was smaller than 0.03 m s^{-1} at all eMOLT stations, while speeds in the lowest ADCP bin at the NERACOOS locations were between 0.025 m s^{-1} and 0.04 m s^{-1}.

The longer term (5-day low-pass filtered) speed magnitudes were larger than the wind-band flows at all stations with most locations having longer term fluctuations almost twice as large as the ones in the wind-band.

3.1.2. Model skill assessment

Modeling the flow around relatively small-scale bathymetric features requires adequate model resolution and accurate bathymetric data. As such, it represents a significant challenge for regional models. The skill of the FVCOM model velocities was assessed by comparing them with the observed velocities from the NERACOOS ADCPs deepest bin and the eMOLT tilt meters.

The model tidal speeds were comparable to observed values with misfits less than 0.02 m s^{-1} at most eMOLT stations (Fig. 3B) except near Grand Manan Island (eMOLT 14), where the model overestimated the tidal flow. The differences between model and observations at the NERACOOS locations were within 0.03 m s^{-1} of the observed values. The largest differences were in more energetic tidal locations like the eastern Maine shelf ($I1$) and Jordan Basin ($M1$).

Model skill in the wind band (Fig. 3C) was good as the largest misfits remained close to 0.01 m s^{-1}. While the percentage difference was relatively large in this band, the speed differences were small and model agreement better than 0.01 m s^{-1} was not expected considering model resolution and instrument noise. Model skill in longer than 5 days band was also generally good with most stations being within the 0.01 m s^{-1} error envelop (Fig. 3D). The largest model misfits were at stations that had larger M_2 tidal errors in areas of steep bathymetric gradients (NERACOOS $I1$, $M1$, and eMOLT stations 6 and 14). Inaccuracies in model bathymetry result in errors in both M_2 tidal speed and residual flows due to tidal rectification.

3.1.3. Bottom flow during storms

The archived FVCOM solution was taken as a best available estimate of the near-bottom velocity. As mentioned in Section 2.1, the depths of the model bottom-most layer varied throughout the domain, so to allow a Gulf-wide description at a standard depth, velocities were estimated at 1 m above bottom (hereafter near-bottom) assuming a law-of-the-wall profile with a roughness length of 0.005 m (consistent with the values used in Butman et al., 2014).

Simulated sediment resuspension was closely associated with storm events and thus the model velocities during storms are most relevant for sediment transport. To characterize energetic events, storms were defined as periods when bottom wave-current stress exceeded 0.1 Pa at WMS (selected as the storm-defining station because of the smaller contribution of tidal stress to the total bottom stress at that location). Based on this definition, storms occurred 12% of the time at WMS. The average near-bottom velocities (1 m from the seafloor) during storm periods (Fig. 4) were larger than the average for the entire study period or for any of the seasonal averages (fall, winter or spring, not shown) along the Maine shelf. The bottom circulation in the GoM is characterized by subregional features that sometimes appear to be disconnected because of the changing depth of the seafloor.

During storms, model skill at the NERACOOS locations was adequate (0.02 m s^{-1} average difference) despite the increased magnitude of the flow. Only NERACOOS velocities were used for comparison during storms as the eMOLT data did not span the entire simulation period. The skill during storm periods suggests that the level of agreement was sufficient for studying sediment transport and redistribution, which primarily occurred during energetic events (even though small concentrations of sediment can be transported after stress falls below 0.1 Pa).

The model predicted spatially coherent, predominantly south-westward near-bottom velocities during storms along the Maine, New Hampshire and Massachusetts shelf in water depths less than 100 m. The predominantly southwestward flow is in a similar direction to the observed average storm wind. Over the central and eastern Maine shelf at water depths shallower than 100 m, there was a near-bottom offshore flow of about 0.06 m s^{-1}, consistent with downwelling associated with winds from the northeast. The flow was mostly along shelf in the western Maine shelf and off Massachusetts with maximum velocities between 0.04 and 0.06 m s^{-1}.
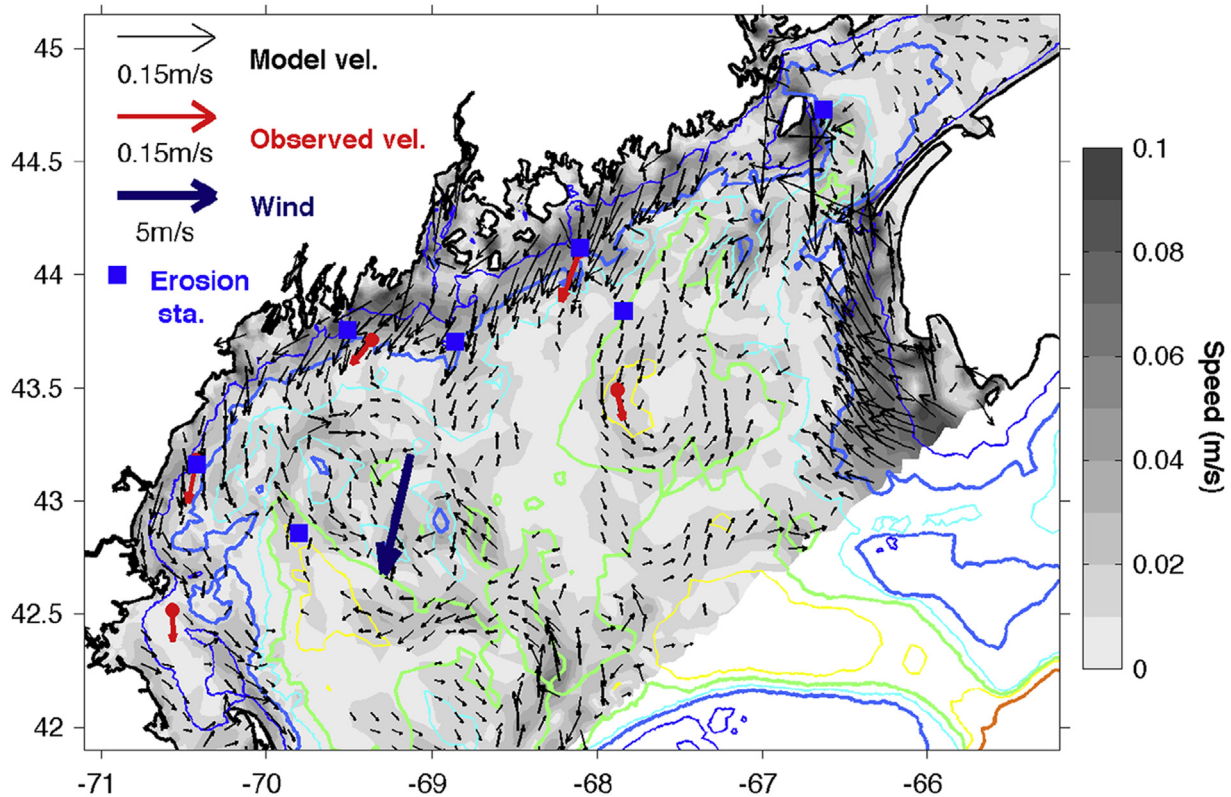
The near-bottom velocity during storms was largest at the entrance to the Bay of Fundy and over the Scotian Shelf, exceeding 0.15 m s^{-1} over the shallow areas around Grand Manan Island. There was a southwestward 0.02–0.04 m s^{-1} flow along Grand Manan Basin in areas deeper than 150 m. The Bay of Fundy gyre depth-averaged flows described in Aretxabaleta et al. (2008) were not easily identified in the model near-bottom velocities. There was a partial connection between the strong tidal residual velocities over the shallow areas around Grand Manan Island and the flow inside Grand Manan Basin that extended to the 150 m isobath. During storms, the northwestward flow along the Scotian Shelf between the 50 and 120 m isobaths was around 0.06 m s^{-1} and generally perpendicular to the average wind direction during storm periods. The general features of the near-bottom circulation in the eastern Gulf and Bay of Fundy region (northwestward flow over the Scotian Shelf, flow along Grand Manan Basin) were consistent with the estimates provided by Lauzier (1967) from the analysis of seabed drifters.

In the deeper part of the Gulf, the model predicted two predominant near-bottom flow features during storms: a 0.04–0.06 m s^{-1} flow from the western part of Georges Basin, through Rogers Pass, into the deeper part of Wilkinson Basin; and a 0.02–0.03 m s^{-1} counter-clockwise gyre that extended throughout Jordan Basin.

3.2. Sediment dispersion

Particles representing the different sediment classes were tracked in the full 3-D velocity fields (Section 2.3). In this study,

Fig. 4. Average model near-bottom velocities (black vectors) and NERACOOS ADCP observations (red vectors) in the western GoM during storms (defined as times when bottom wave-current stress in excess of 0.1 Pa at WMS). Grayscale indicates speed (m s^{-1}) and only velocity vectors larger than 0.01 m s^{-1} are shown. The average wind from NDBC Buoy 44005 is included in dark blue. The 5032(blue), 100 (thick blue), 150 (light blue), 200 (thick orange), 250 (yellow), and 500 (thick red) m isobaths are shown.

the focus is on the mud classes (assumed to be in aggregated form), as they better represent the size and vertical settling of the *A. fundyense* cysts in the water column. The total mud concentration (8 μm and 2 μm classes) was calculated, and particles were released according to the estimated time-varying concentration and tracked from their release time until deposition on the seafloor or until the end of May, whichever came first. The vertical and horizontal sediment distributions are presented as the percentage of the total sediment suspended from each station. The percentages must be scaled by the total sediment concentration (Fig. 2, Table 1) to quantitatively compare total redistribution between stations.

3.2.1. Vertical distribution during transit

Particles representing resuspended sediment concentration were found throughout the water column, generally increasing with depth and with larger percentages near the bottom (Fig. 5). The vertical distribution was estimated as the cumulative percentage of particles found at a depth in the water column over the entire area where material from a specific source was found and only included particles before they redeposited.

$$M(Z_j) = \frac{1}{N}\sum_i M(X_i, Y_i, Z_j \leq Z_i < Z_j + \Delta Z_j, T_i) \qquad (1)$$

where $M(Z_j)$ was the mass of sediment in depth bin j (bin thickness, ΔZ_j) and N was the total mass, $N = \sum_i M(X_i, Y_i, Z_j, T_i)$. Eq. (1) captures the overall vertical dispersion of the particles, but does not represent the vertical concentration at any specific location or the initial distribution at the source location.
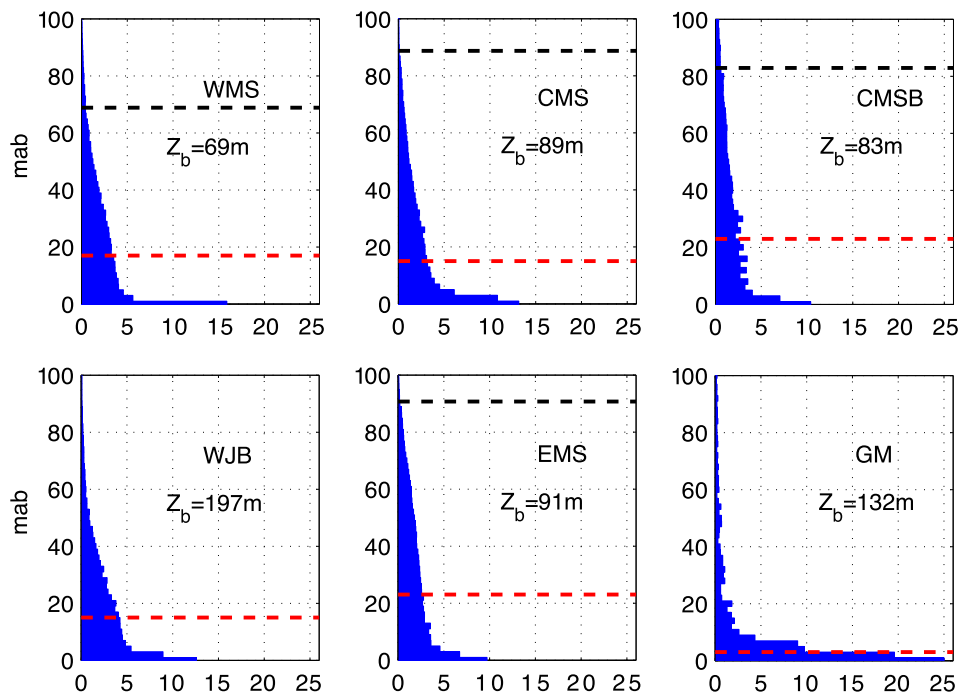
The percentage of total transported sediment that was found at each vertical level varied from station to station with locations in water depths less than 100 m having a larger percentage of

sediment at shallower depths. The largest percentage encountered less than 2 m from the bottom was sediment resuspended at GM (25%). The near-bottom percentage at the rest of the stations ranged from ∼8 to 13% in the bottom bin (2 m). At every station, at least half of the concentration was found within 25 m above the bottom. In all stations shallower than 100 m, the resuspension events, caused predominantly by storms, placed significant sediment concentrations into most of the water column.

The profile of material resuspended from WJB showed higher percentages in the bottom 50 m of the water column which is consistent with the presence of a nepheloid layer in the deep basin. However, the total concentrations resuspended from WJB were minimal (average mud concentration of 2×10^{-3} mg l^{-1} over the bottom 50 m, Table 1) because of the small resuspension estimated in (Butman et al., 2014). WJB was located on the western side of Jordan Basin; bottom stresses on the eastern side of the basin were 2–3 times larger (Butman et al., 2014) and larger resuspension was expected in that area. Concentrations of suspended particulate material from water samples in Jordan Basin (Pilskaln et al., 2014) were 2–3 orders of magnitude larger than the simulated resuspended concentrations at WJB. The inconsistency suggests that to maintain the observed nepheloid layer (1) material was advected from other locations (likely the eastern side of the basin), (2) local resuspension was underestimated, and/or (3) sediment flocculation/deflocculation affects settling speeds of both locally resuspended and newly advected material.

3.2.2. Horizontal distribution after redeposition

The distribution of eroded sediment that settled after one resuspension event depended on initial location (Fig. 6). Most of

Fig. 5. Vertical distribution of simulated sediment (mud) concentration during transit (before redeposition) as percentage of total sediment available for transport at each source station. The vertical axis is depth above the bottom (m). The horizontal dashed black line corresponds to the depth at the source station (Zb) for stations with bottom depth shallower than 100 m. The dashed red line corresponds to the depth at which 50% of the sediment was found above and 50% below. Depth bins are 2 m wide.

the sediment, especially sand (not shown), settled in the proximity of the release location (less than 20 km away from the source), but some of the eroded mud (less than 4%) traveled distances greater than 100 km. Particles tend to spread more in the along-isobath direction than in the cross-isobath direction, as expected given the tendency for the flow to follow topographic contours.

At GM (Fig. 6A), most of the resuspended sediment remained in the Bay of Fundy in the area where the recirculation gyre (Aretxabaleta et al., 2008, 2009) helps retain sedimentary particles in the water column. A small percentage ($<1\%$) exited and was carried southwestward along the eastern Maine coast with some ($\sim 0.002\%$) reaching the station CMSB. This advective pathway is highlighted in Pilskaln et al., 2014) as potentially important for the transport of cysts within the benthic nepheloid layer. Sediment originating from EMS (Fig. 6B) traveled along-shelf, preferentially southwestward, with $\sim 2\%$ of the total eroded mass being redistributed to distances greater than 100 km. At EMS, sediment was resuspended for several months (Fig. 2), resulting in a quasi-continuous source of material and causing the most extensive sediment redistribution. At WJB (Fig. 6C), the majority of the sediment remained in the vicinity of the source ($>99.9\%$ within 10 km). At CMSB (Fig. 6D), sediment was distributed both along- and cross-shelf, and a small percentage of particles ($\sim 3\%$) were redistributed in the western Gulf of Maine southwestward of CMSB in areas deeper than 100 m. The majority of the particles ($\sim 95\%$) from CMSB remained in the area where sedimentary cyst concentrations larger than 500 cysts cm^{-3} were found during 2011 (Anderson et al., 2014). Sediment from CMS was mainly transported along-shelf with both southwestward and northeastward redistribution (Fig. 6E). At WMS, the redistribution was more substantial and material from this station traveled significant distances along-shelf.

The percentage of total eroded material that traveled beyond successively larger concentric circular areas provided a quantitative estimate of sediment export from each station (Fig. 7). More than half of the sediment eroded from WMS and EMS traveled distances farther than 10 km, while between 30 and 40% of the

material from CMS, CMSB and GM exceeded that distance. The percentage of sediment going beyond 20 km from the source was largest at WMS ($\sim 60\%$). Between 10 and 20% of the material from CMS, CMSB, and GM went beyond 20 km from the source before resettling, while more than a third of sediment from EMS exceeded that distance. Trace amounts (less than 0.1%) of the very small amount of eroded material at WJB (Table 1) traveled farther than 20 or even 10 km from WJB. The percentages of sediment traveling more than 50 km were smaller (20% at WMS, 12% at EMS, around 5% at CMSB and GM, and 2% at CMS). Finally, sediment that traveled distances longer than 100 km before redepositing was less common with only three stations having exceeded 1%: 3.7% from WMS, 2% from EMS and 1% from GM. Only 0.1% of sediment from CMSB traveled beyond 100 km.

The difference between source depth and resettling depth quantified the relative importance of onshore–offshore transports (Fig. 8). Most of the sediment redistribution was estimated to occur in a depth range within 40 m of the depth of the source location. The largest offshore export of sediment was from GM, where greater than 20% of the resuspended sediment resettled between 40 and 70 m deeper than the source depth (predominantly over Grand Manan Basin). Sediment from the western and central Maine shelf stations had a net onshore displacement (i.e., settling in shallower water depths than the source) while there was a net offshore export of sediment from the rest of the stations. The second largest offshore export was estimated for CMSB, where more than 10% of the sediment eroded from that location resettled in depths 40–60 m deeper than the source depth.

3.2.3. Seasonal redistribution

Seasonal variation in redistribution could potentially affect the cyst dynamics in the GoM. The relative contributions during each season to the total onshore/offshore transport (Fig. 8) varied from station to station. Sediment from WMS, CMS, and CMSB was primarily advected during winter with almost no transport during fall. In contrast, particles from WJB were mostly redistributed
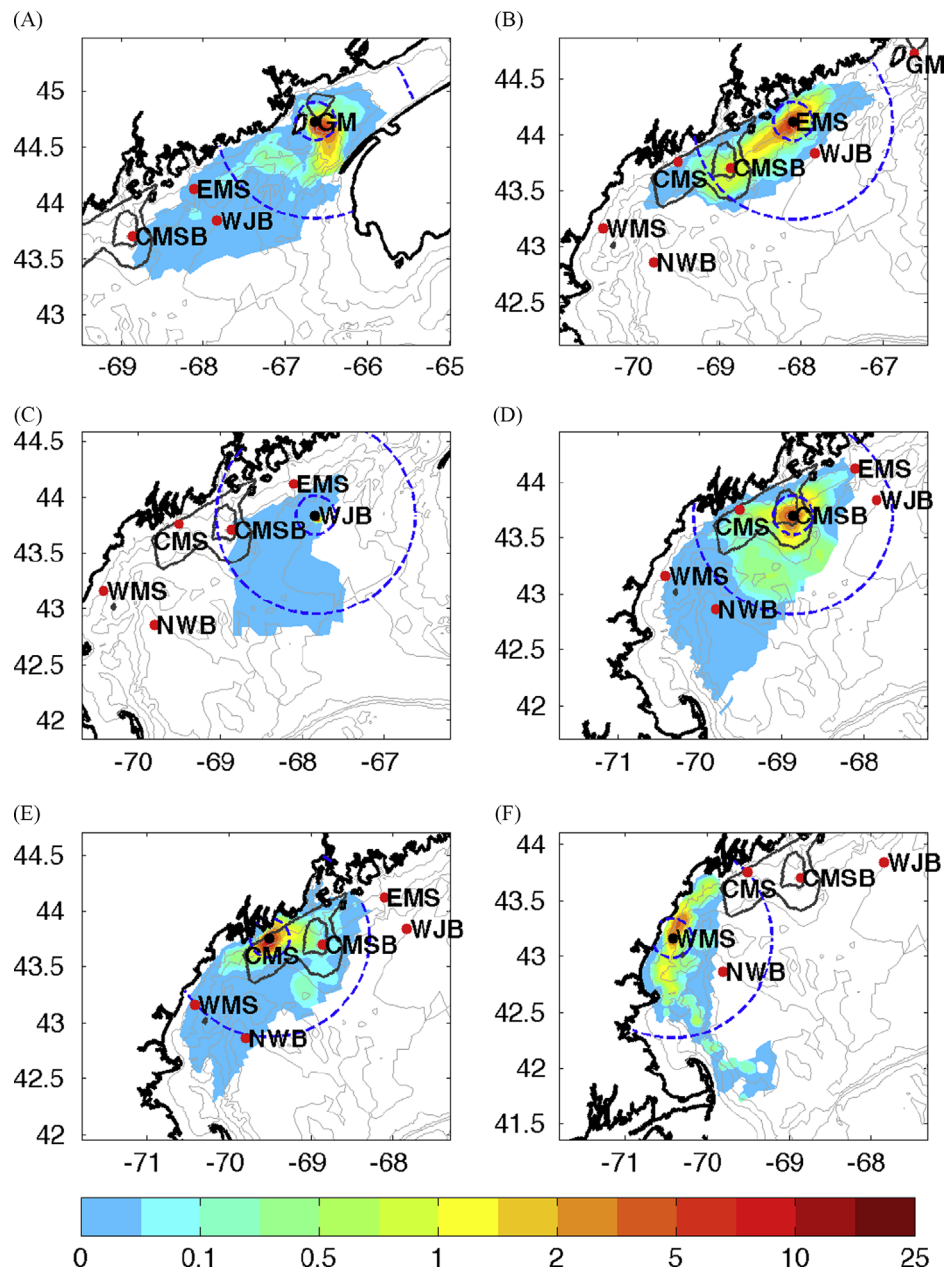
Fig. 6. Modeled spatial distribution of resettled mud concentration originating from each station with resuspension (the model predicted no erosion at NWB), as a percentage of total eroded sediment. Only positions where particles were found are shown (colored area). Note the color axis is logarithmic. Circles with radius of 20 and 100 km around each station are included in dark blue. The 2011 cyst concentration contours of 500 and 1000 cysts cm^{-3} are shown in dark gray. The 50, 100, 150, and 200 m isobaths are also shown.

during spring. As sediment from EMS was available for transport during most of the study period, it was advected during both winter and spring. At GM, sediment was transported during each of the three seasons, a result of recurrent resuspension by the tides, but there was enhanced offshore transport of sediment during spring with a larger fraction settling between 50 and 70 m deeper than the source depth.

As the particle redistribution during fall was minimal at most stations, we focused the seasonal comparison in winter (December–March) and spring (April–May) (Fig. 9). During winter, material resuspended from GM predominantly remained in the Bay of Fundy gyre area with only a small percentage (< 1%) being exported along the MCC path (Fig. 9A). In contrast, during spring, a larger fraction (~5%) was exported out of the Bay (Fig. 9B) with material first being transported south and then southwestward along Grand Manan Basin. During winter, sediment from EMS

(Fig. 9C) was redistributed along-shelf almost evenly in both directions with small percentages (~2%) traveling past CMSB. During spring (Fig. 9D), material from EMS was predominantly transported southwestward with a larger fraction of the total sediment (~4%) reaching the vicinity of CMSB and CMS. During winter, sediment from CMSB (Fig. 9E) was redistributed in both along- and cross-shelf directions with a considerable fraction (~1%) traveling southward offshore to areas deeper than 100 m.

During spring (Fig. 9F), the redistribution from CMSB was more along-shelf, traveling between the 80 and 120 m isobath. While sediment was resuspended during both winter and spring at GM and EMS (Fig. 2), most of the sediment from CMSB was resuspended during a single storm at the end of December and thus the winter field represented most of the redistribution over the study period. Transport of sediment resuspended from CMS and WMS (not shown) was mostly southwestward along-shelf during spring,

a result of the net westward flow (Fig. 4), and in both along-shelf directions during winter.

3.2.4. Sensitivity to settling velocity

Two critical factors affected the redistribution of sediment: (1) the amount of time that the particles remained in the water column; and (2) the vertical location of particles in the water column, as near-surface flow tends to be more energetic. The assumed vertical settling velocity of the simulated sediment has an effect on both the travel time and vertical distribution of the particles.

Three values of vertical settling velocity (1, 0.1, and 0.04 mm s^{-1}) were tested and the comparison is shown for station
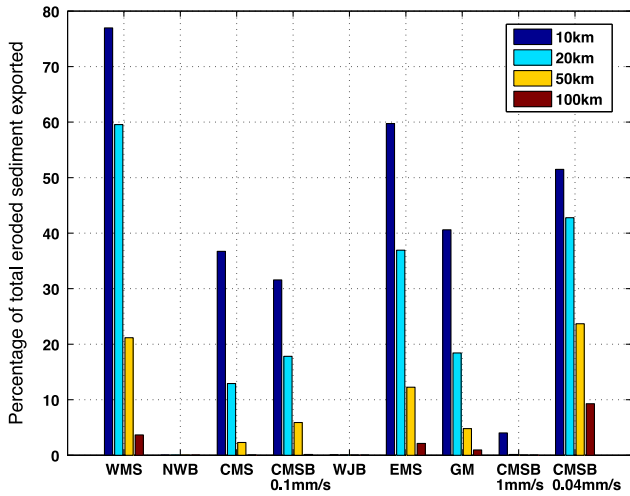

Fig. 7. Percentage of total eroded sediment from each station exported beyond the boundaries of a circle of 10 km (dark blue), 20 km (light blue), 50 km (yellow), and 100 km (red) radius centered around the released location. (Circles with radius of 20 and 100 km are shown in Fig. 6). The settling speed of the simulated particles was 0.1 mm s^{-1} unless indicated otherwise.

CMSB (Fig. 10A, Fig. 6D, and Fig. 10B). The fastest settling (1 mm s^{-1}) resulted in virtually no transport of material outside the vicinity of the source location (less than 20 km) and the distribution pattern was quite similar to the results obtained for sand (not shown) with a slightly higher settling speed (8 mm s^{-1}). The slowest settling velocity resulted in a redistribution of material over a large part of the western GoM with small percentages being exported offshore and redepositing over Wilkinson Basin. However, even with slow settling velocities, the bulk of the material remained in areas close to the source. While only 4% of the material eroded from CMSB sinking at 1 mm s^{-1} traveled beyond 10 km, over 30% exceeded that distance with the nominal 0.1 mm s^{-1} sinking, and over half of the total eroded mass when the slow sinking was considered (Fig. 7). Almost 10% of particles sinking at 0.04 mm s^{-1} traveled distances longer than 100 km from CMSB, almost 2 orders of magnitude more than with the nominal sinking speed. Similar redistribution extremes were observed at other locations (not shown).

3.3. Redistribution timescales and connectivity

Sediment redistribution maps (Figs. 6,9,10) characterize the spatial spreading of material from the source, but when used to determine effective connectivity between locations, the potential flow and tracking uncertainties (e.g., model errors, changing tracking behavior doing long intervals) must be considered. Because Lagrangian pathways reflect integrals of the velocity field, transport errors accumulate in time. To provide an estimate of the time scales associated with the sediment redistribution, the shortest time that particles spent in transit to each location was calculated (Fig. 11). Some material from GM exited the Bay of Fundy in periods of 1–2 days (Fig. 11A). Sediment from GM was transported faster along two routes: a northern path southwestward along the eastern Maine shelf during winter (Fig. 9A) and a southern path along Grand Manan Basin during spring (Fig. 9B). After 5 days of rapid transport, particles from GM slowed, taking around 15 days to reach EMS and WJB, and in excess of 25 days to
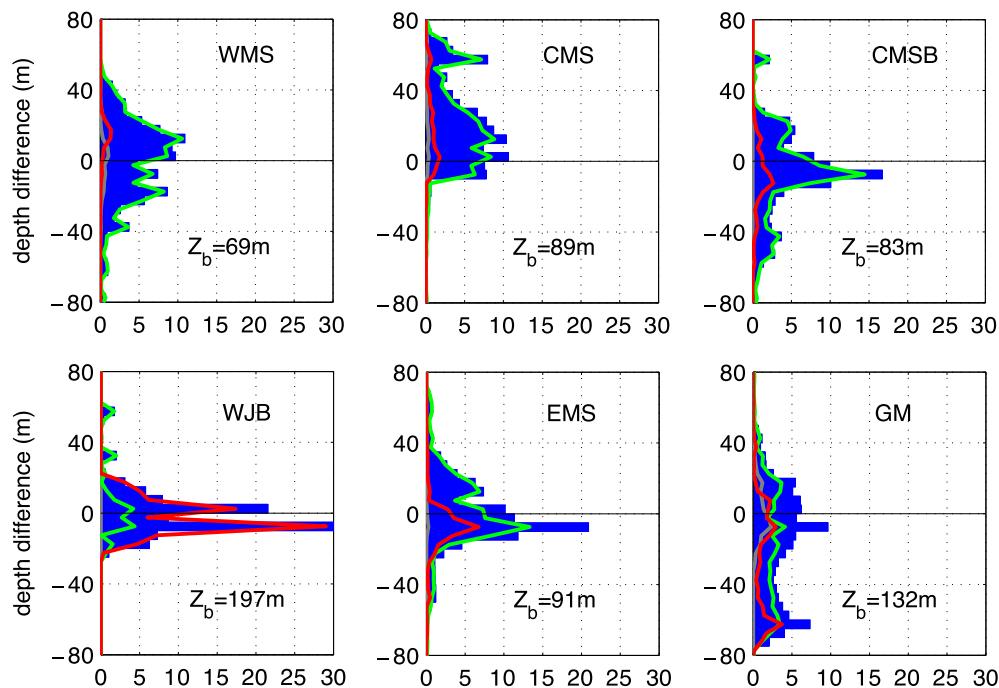

Fig. 8. Percentage of total redistributed sediment versus depth where particles settled (difference from source depth). Zero implies that particles resettled at the same depth as the source station. Positive (negative) depths implies onshore (offshore) displacement. Depth bins are 5 m wide. Solid lines indicate seasonal contributions: fall (gray), winter (green), and spring (red).

reach CMSB. Particles from EMS (Fig. 11B) were redistributed faster, with most of the influenced area being reached in less than 10 days, and with particles covering much of that area within 2 days. Particles from EMS arrived at CMSB within 3 days, while taking longer than 20 days to reach WJB and CMS. Particles from CMSB (Fig. 11C) followed two main paths: a narrow along-shelf band between 80 and 120 m water depth and a broader slower offshore transport. Particles from CMSB needed at least 10 days to arrive at WMS and EMS, reached CMS in less than 2 days and needed longer than 30 days to transit to the NWB station. Some particles from WMS (Fig. 11D) traveled distances longer than 50 km in less than one day, predominantly along-shelf during

storms. Sediment from WMS traveled east of Cape Cod in 5–10 days.

While redistribution fields (Section 3.2) provided information about distance traveled by sediment from each location, the redistribution of cyst-containing sediment to other stations are examined using estimates of station connectivity (Table 2). The destination area was chosen to be a 20 km radius circle around each source location because the minimum distance between stations (EMS and WJB) was around 40 km. Smaller (6 km radius) and larger (50 km radius) choices of destination areas were also tested (not shown). The 6 km radius area followed the size used in other connectivity studies (Mitarai et al., 2009; Li et al., 2014), while 50 km was tested to cover
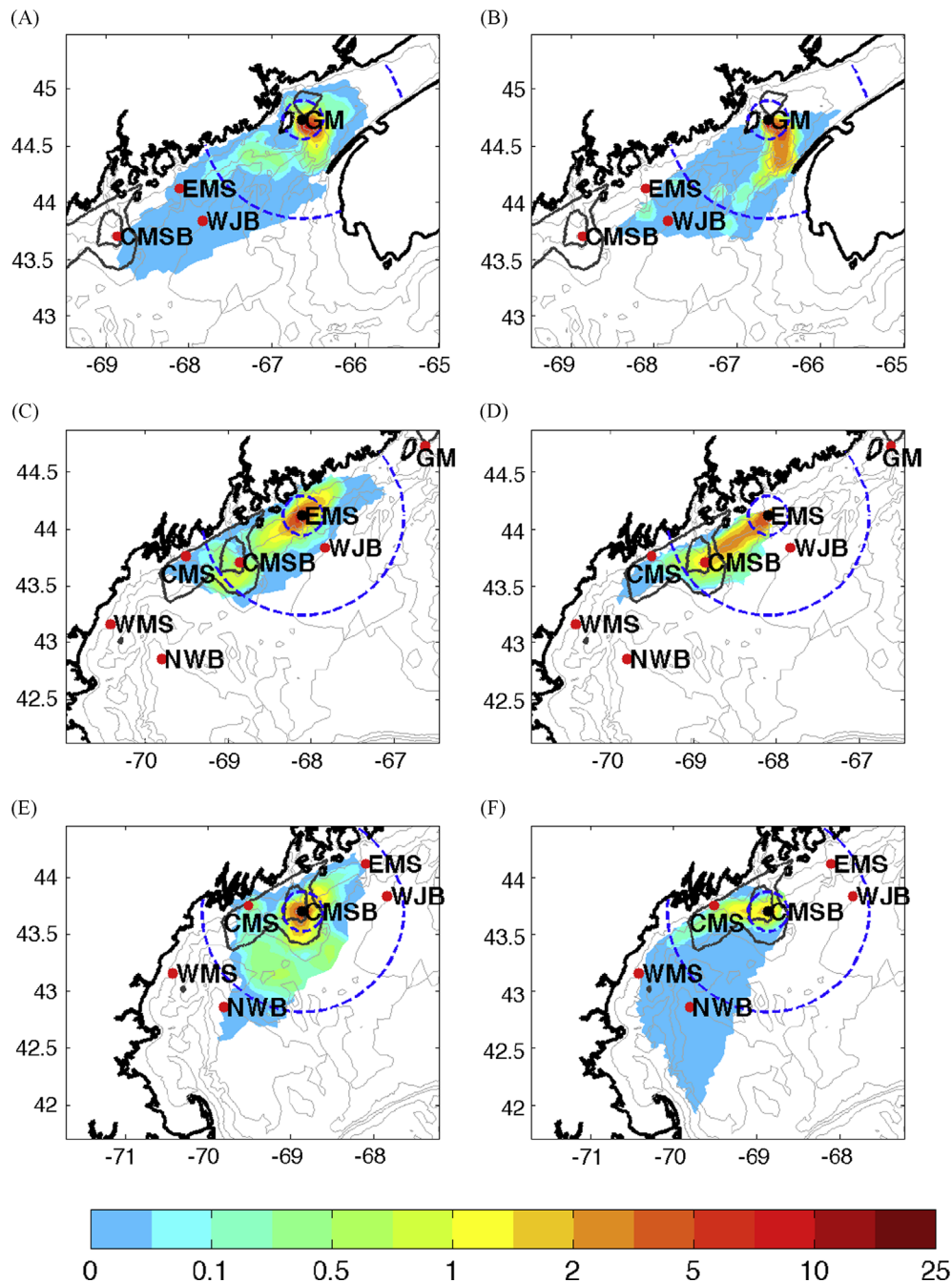
Fig. 9. Redistribution percentage during winter (December–March, left panels) and spring (April–May, right panels) for stations: GM (A, B); EMS (C, D); and CMSB (E, F). The shown values are percentages of the total sediment resuspended during each period (e.g., April–May for spring). The 2011 cyst concentration contours of 500 and 1000 cysts cm^{-3} are shown in dark gray.
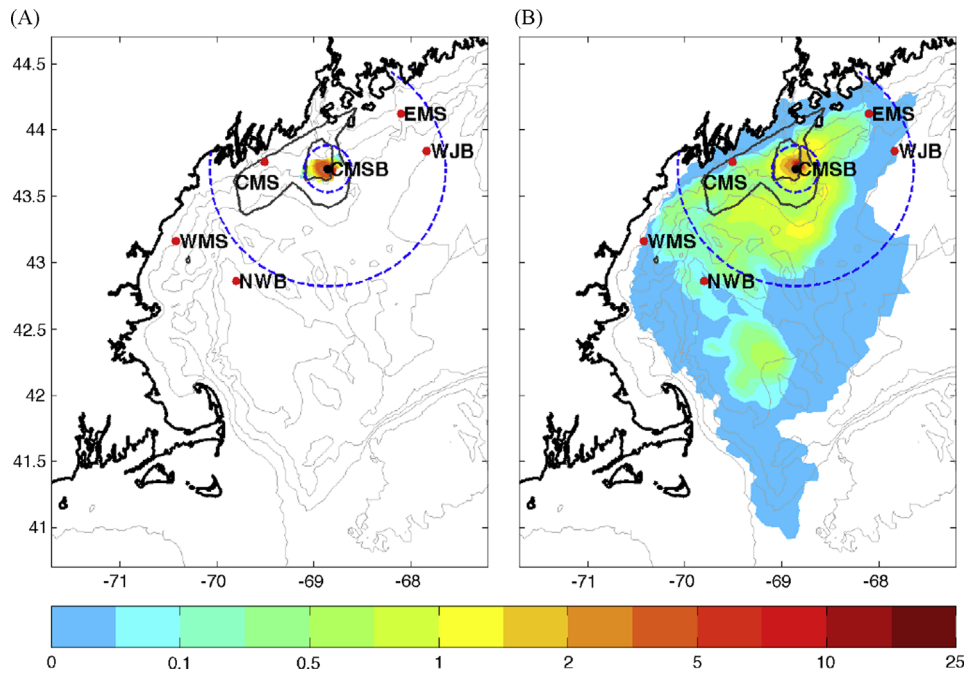
Fig. 10. Redistribution of sediment from CMSB with different vertical settling velocities: (A) 1 mm s^{-1}; and (B) 0.04 mm s^{-1}. See Fig. 6D for redistribution with settling velocity of 0.1 mm s^{-1}.

the majority of the shallower than 100 m areas of the GoM. The estimated redistribution percentage remaining locally decreased in the 6 km case and increased in the 50 km case, but the relative percentages remained about the same. Ultimately, 20 km was chosen as it provided sufficient coverage while avoiding overlapping areas. Table 2 provides an estimate of the connectivity between different areas in the GoM and BoF. As no material was eroded from NWB, that location was only considered as a destination. At stations CMS, CMSB, WJB, and GM more than 80% of eroded material was redeposited within 20 km, while at stations WMS and EMS 40% and 63%, respectively, was redeposited within 20 km. While EMS provided sediment to several studied destinations, WMS exported half of its material outside the area characterized by the 7 locations, a result of WMS being on the western edge of the study area, and the generally southwestward flow along the Maine shelf.

4. Discussion

The concept of open/closed populations (Mora and Sale, 2002; Cowen et al., 2006, 2007) can be extended to the redistribution of sediment. Following the ecological definition, the material from a closed population is primarily caused by local processes, while an open population receives most of its material from other locations. In general most of the locations in the GoM could be considered predominantly closed for the horizontal and temporal scales considered in this study. The balance between number and size of source/destination locations and the level of complexity remains a difficult issue to resolve (Mitarai et al., 2009; Li et al., 2014). However, our goal was to characterize general areas for which erodibility and sediment concentration was available, and thus only the 7 locations with erodibility measurements were considered. Stations WMS and EMS exported more than 50% of their resuspended sediment concentrations to areas outside the 10 km radius area (Fig. 7) but the maximum percentages reaching the 20-km radius around adjacent stations were 6.4% from EMS to CMSB and 3.6% from CMSB to CMS.

EMS was the station with the largest total resuspended mass (Fig. 2, Table 1) and also had the second smallest percentages

remaining locally (Table 2). Therefore, EMS could be considered as one of the main export areas of the GoM (most open "population"). A similar case could be argued for GM and WMS, but only small (none in the WMS case) percentages of material from these stations reached any of the other locations. WMS was at the western end of the domain and transport from that station, especially during storms, was westward. Material exported from WMS could potentially settle in downstream areas such as Massachusetts Bay and Georges Bank, although the percentages would likely be low due to the long distances involved. The three stations with largest percentages of exported sediment (WMS, EMS and GM) also had the largest fraction of sand (Table 1), consistent with their strong average bottom stress (Fig. 2) and were areas of enhanced flow, especially during resuspension events.

CMSB, located in the center of the study area, was connected with a largest number of destination locations; material resuspended at CMSB reached WMS (almost none), NWB, CMS, and EMS. It also received material from the largest number of stations, most notably EMS, but also GM and CMS. Thus, CMSB could be considered a partially open "population" that affected nearby stations but was also influenced by them. The modeled bottom flow in the vicinity of CMSB showed considerable seasonal variability, with flow during fall converging to the source location (not shown) while strong offshore (southwestward) velocities were predicted during storm periods (Fig. 4). The model predicted near-bottom convergence during fall at CMSB that might facilitate the observed enhanced cyst concentration as slowly sinking particles would tend to accumulate in the area. The flow associated with storms could influence the redistribution of sediment containing cysts during the critical spring germination period.

The connectivity calculations suggest that the area surrounding the WJB station received material from local resuspension and from stations in shallower areas of the shelf (EMS, GM). Another potential source of suspended material for WJB is the eastern side of Jordan Basin where predicted wave-current bottom stresses are significantly higher (Butman et al., 2014). Unfortunately, no erodibility information is available from the eastern side of the basin. However, material resuspended from eastern Jordan Basin could be transported by the counterclockwise gyre (Fig. 4; Brooks, 1985;
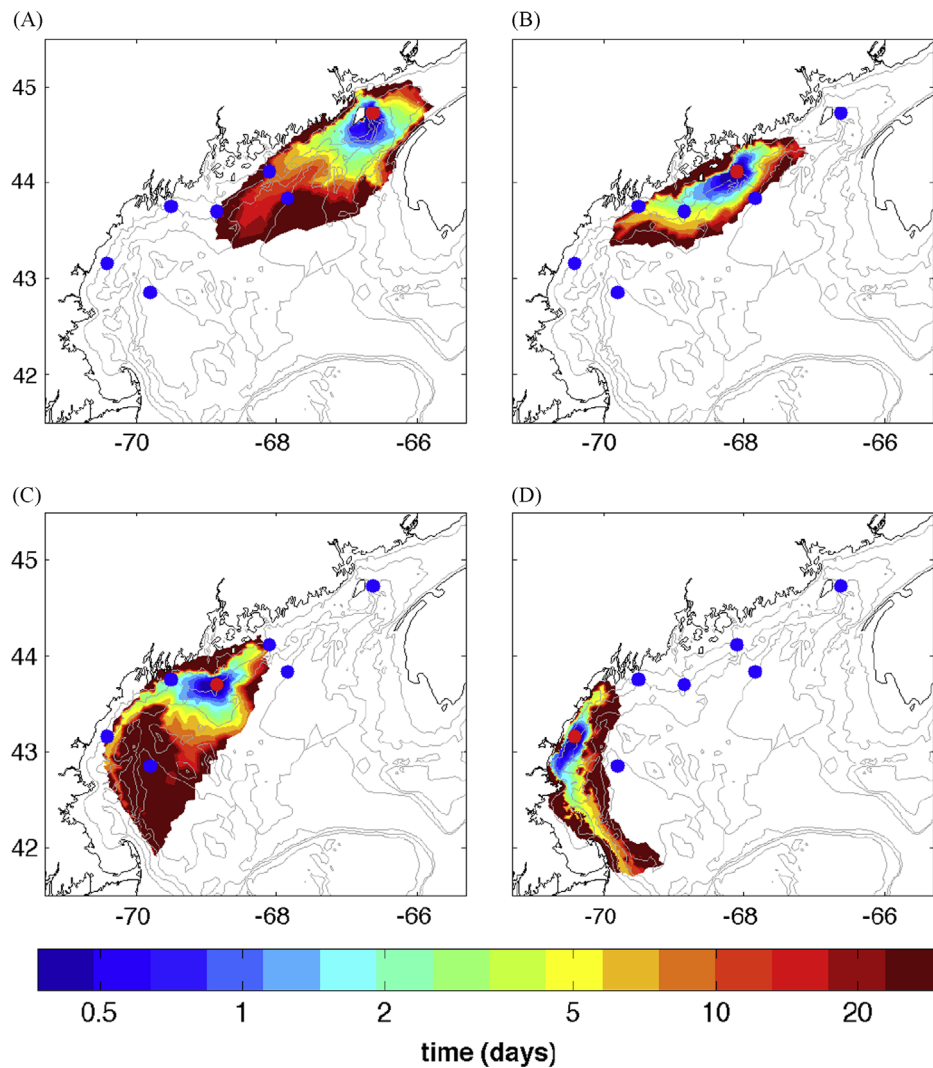
Fig. 11. Spatial distribution for the shortest time (in days) particles spent to reach each location. Particles were resuspended from (A) GM; (B) EMS; (C) CMSB; and (D) WMS. Source stations indicated with red dots and the rest of the stations with blue dots. Colorbar shows time in days in a logarithmic scale.

Pettigrew et al., 1998) to the western and central parts of the Basin. Beam attenuation observations (see Fig. 2 of Pilskaln et al., 2014) are consistent with enhanced suspended sediment higher in the water column, likely associated with resuspension in the eastern side of the Basin. In any case, quantitative partitioning amongst the various sources of suspended material at WJB awaits further study.

To provide an estimate of the potential for cyst redistribution among the various regions, the percentage from the original cyst concentration for 2010 and 2011 from each of the stations into the remaining stations was calculated (Table 3) using the following expression:

$$P_i = \frac{C_i - e_i + \sum_j d_i^j}{C_i} \times 100 \qquad (2)$$

where the percentage, P_i, was given by the ratio between the original cyst concentration at station i (C_i), the cysts eroded at that location (e_i) and the sum of the deposition of cysts, d_i^j, from each source j into the destination i.

The largest cyst concentration decrease (4.5% in 2010 and almost 7% in 2011) was estimated for CMSB as it received a large percentage of sediment from EMS that contained lower cyst concentrations than the ones measured at CMSB. The largest

Table 2
Percentage of material transported from each source station into each destination location for the entire period (October–May). The destination area is chosen to be a circumference of 20-km radius around each of the stations.

Start	Destin.							
	WMS	NWB	CMS	CMSB	WJB	EMS	GM	total
WMS	40.5	0.0007	0.0	0.0	0.0	0.0	0.0	40.5
NWB	0.0	0.0	0.0	0.0	0.0	0.0	0.0	0.0
CMS	0.08	0.0	87.1	0.9	0.0	0.002	0.0	88.1
CMSB	0.002	0.015	3.6	82.2	0.0	0.2	0.0	85.9
WJB	0.0	0.0	0.0	0.0	99.97	0.0	0.0	99.97
EMS	0.0	0.0	0.3	6.4	0.4	63.1	0.0	70.2
GM	0.0	0.0	0.0	0.002	0.08	0.1	81.6	81.8

estimated cyst concentration increase was at WJB and CMS in 2010, which was caused by cysts from EMS to WJB and from CMSB to CMS. The results suggest that only a small fraction of the cyst concentration (usually less than 1%) was affected by the redistribution of sediment from the considered locations. If more stations or shorter distances between stations were considered then the percentage exchange between stations would increase. The eroded depth that provided sediment to the water column was on the order of 1 mm (Butman et al., 2014), while the cyst

Table 3

Cyst redistribution assuming destination stations cover the entire GoM (i.e., stations are representative of large areas and every resuspended cyst is assigned to the nearest destination location). The first and fourth rows include the cyst concentration (cysts cm^{-3}) measured in the top 1 cm of bed during the October 2010 and October 2011 cruises at each of the stations. The second and fifth rows represents the cyst concentration at each destination station in 2010 and 2011 (assuming same redistribution pattern), respectively. The percent of sediment redistributed from each source was multiplied by the source cyst concentration and summed up for each destination area (20 km radius). The third and sixth rows are the percentage change from the initial concentration.

Stat.	WMS	NWB	CMS	CMSB	WJB	EMS	GM
Initial 2010	1645	115	930	1827	148	938	1312
Final 2010	1644.3	115.3	966	1745	153	940	1312
% change	−(<0.1%)	0.3%	3.8%	−4.5%	3.7%	0.20%	0%
Initial 2011	190	32	912	1250	172	246	323
Final 2011	190.7	32.1	923	1163	172.6	248	323
% change	0.4	0.7%	1.2%	−6.9%	0.3%	0.9%	0%

inventory extended over the upper few centimeters of sediment (Anderson et al., 2014). The vertical distribution of cysts in the sediment exhibited significant temporal variability (Shull et al., 2014) with increased concentration in the top millimeter after deposition and reduced concentration during germination. Thus, the timing of the resuspension events could also alter the cyst exchange between different locations. In the present cyst redistribution calculations, the cyst was assumed to be well-mixed in the top centimeter, but increased numbers in the top millimeter after deposition could alter the calculated percentage.

The cyst redistribution estimate was computed between a few source/destination pairs that represent a small fraction of the total sediment being redistributed during the study period. A full three-dimensional sediment transport simulation would be needed to provide adequate cyst redistribution estimates. Accordingly, the main focus of the current simulations was to characterize the spatial and temporal connectivity between different areas of the GoM from a sediment perspective, not to predict absolute changes in cyst concentrations (although a first approximation was provided in Table 3).

Several processes not included in the simulations could increase the reported transport distances. The Lagrangian simulations provided estimates of distance traveled by the sediment from each resuspension event. However, when the sediment redeposited in a new location, those particles were not resuspended by subsequent events. Additionally, turbulent diffusivity (not included in the tracking procedure) would tend to maintain particles in suspension, increasing lateral transport. Therefore, the calculated particle redistribution represents conservative values for material export from any of the specified sources and the exchange is expected to be more extensive than calculated here. The results were estimated for a particular year (2010–2011), but substantial interannual variability has been described in the GoM in circulation (Li et al., 2014), storm frequency and intensity (Butman et al., 2014), and cyst distribution (Anderson et al., 2014).

Sediment particles (mud) in the water column are assumed to be flocculated but the process of aggregation/disaggregation could alter the sinking speed of particles in the water column resulting in significantly different redistribution patterns and distances. For instance, the percentage of sediment traveling distances in excess of 50 km from the source at CMSB increased from 5% with a nominal 0.1 mm s^{-1} sinking rate to 25% with a settling speed of 0.04 mm s^{-1} (within the range of settling velocities of flocculated particles described in Winterwerp, 2002) with about one percent of the total slowly settling sediment traveling to stations WMS, EMS and NWB.

The particle redistribution results were estimated using the best publicly available model hindcast to provide qualitative insight into particle dynamics. Despite the fact that FVCOM near-bottom flows exhibited small differences when compared with observations in some areas of steep topography, two factors suggest that the redistribution results qualitatively reflect particle redistribution: (1) sediment was predominantly resuspended during storms and the mean model flow during those times exhibited good skill (Fig. 4); (2) the majority of the particles traveled small distances from the source associated with near-bottom flow typically less than a few centimeter per second and the magnitude of both model and observed flows was small (Fig. 3).

5. Summary and conclusions

In the Gulf of Maine, *A. fundyense* cysts are formed at the end of spring/summer blooms, and subsequently sink down to the underlying sediment. Bottom stress caused by waves and tides result in resuspension of sediment and associated cysts during winter and spring. The resuspended material can be distributed throughout most of the water column, but concentrations are generally higher near the seafloor. This material can potentially be transported throughout the Gulf through advection. The archived model velocity estimates were within 0.02 m s^{-1} of observations during storm periods. Numerical particles were released in the model flow to estimate dispersion and redistribution of sediment. The simulated particles included a settling velocity of 0.1 mm s^{-1} for both mud (assumed to be aggregated) and *A. fundyense* cysts. Sinking speed was a critical factor controlling redistribution and the sensitivity to a range of sinking speeds was examined.

Erodibility, sediment fraction and bottom wave-current stress described by Butman et al. (2014) were used to calculate sediment concentrations in the water column. The majority of the resuspended material remained in the vicinity (within 20 km) of the source locations; between 10 and 40% of material from stations shallower than 150 m (except for the western Maine station) traveled beyond 20 km. One percent or more of the resuspended sediment traveled distances longer than 100 km at three stations (3.7% from the western Maine station, 2% from eastern Maine, and 1% from the Bay of Fundy). The particle trajectories were influenced primarily by the southwestward flow associated with storm winds from the northeast during winter and spring, in addition to the MCC during spring. Trace amounts (0.002%) of sediment from the Bay of Fundy were able to reach the central Maine shelf before settling, but most of the material was deposited in the area at the entrance to the Bay and along Grand Manan Basin. The eastern Maine shelf was the largest exporter of material, with maximum suspended sediment concentration associated with strong bottom stress and energetic flow resulting in a significant concentration being transported westward to the central Maine shelf. The central Maine seed bed location was the main exporter of sediment to deeper areas of the Gulf and provided sediment to the largest number of stations, but its influence was limited in this simulation as most of the sediment eroded from this station originated from a single storm event. There was no resuspension estimated at the northern Wilkinson Basin station but was a

recipient of material from shallower stations. Suspended sediment from the western Jordan Basin station was found in characteristic nepheloid layers, although in much smaller concentrations than observed (Pilskaln et al., 2014). The sediment from the central and western Maine shelf was predominantly transported westward along-shelf with little influence on the remaining stations. Sediment redistribution was active on time scales that ranged from 1 to 2 days at stations where sediment export was strong to 20–30 days in less energetic areas. Interannual variability in the circulation and number of storms (Butman et al., 2014) could affect the exchange of material between the different subregions.

The general characteristics of the spatial redistribution is expected to be relatively robust since the velocity field during storm periods showed good skill and storms were the dominant process causing resuspension and initiating the transport of sediment. However, the uncertainties found in the velocity fields (Section 3.1.2), the substantial seasonal variability (Section 3.2.3), the sensitivity to settling velocity (Section 3.2.4), and factors related to sediment resuspension (e.g., erodibility, bottom stress, sediment fraction) could alter the estimated redistribution percentages. We have identified the concentration and settling speed of sediment in the water column, the timing of storms, and the circulation features as being critical to the extend of sediment redistribution, but evaluating the relative importance of all the factors affecting transport in the Gulf is beyond the scope of the current study. The estimated redistribution was based on the trajectories from single erosion/deposition events without the possibility of re-eroding the deposited particles and without the effects of enhanced near-bottom turbulent mixing, and thus the calculated percentages probably underestimate sediment exchange in the Gulf of Maine.

The magnitude of the calculated cyst redistribution was small and because the eroded sediment depth was on the order of 1 mm, unlikely to alter the cyst inventory in the upper several centimeters of sediment except maybe during periods of very high cyst concentration near the sediment surface following cyst deposition. The main contribution from this study is the description of the limited interconnectivity between locations and a first step toward the characterization of the spatial and temporal variability of the sediment dynamics in the Gulf of Maine.

Acknowledgments

Any use of trade, firm, or product names is for descriptive purposes only and does not imply endorsement by the U.S. Government.

References

Anderson, D.M., Keafer, B.A., Kleindinst, J.L., McGillicuddy, D.J., Martin, J.L., Norton, K., Pilskaln, C.H., Smith, J.L., 2014. *Alexandrium* cysts in the Gulf of Maine: time series of abundance and distribution, and linkages to past and future blooms. Deep-Sea Res. II 103, 6–26.

Anderson, D.M., Lively, J.J., Reardon, E.L., Price, C.A., 1985. Sinking characteristics of dinoflagellate cysts. Limnol. Oceanogr. 30, 1000–1009.

Anderson, D.M., Stock, C.A., Keafer, B.A., Bronzino, A., McGillicuddy, D.J., Keller, M.D., Thompson, B., Matrai, P.A., Martin, J., 2005a. *Alexandrium fundyense* cyst dynamics in the Gulf of Maine. Deep-Sea Res. II 52, 2522–2542.

Anderson, D.M., Townsend, D.W., McGillicuddy, D.J., Turner, J.T., 2005b. The ecology and oceanography of toxic Alexandrium blooms in the Gulf of Maine. Deep-Sea Res. II 52, 19–21.

Anderson, D.M., Wall, D., 1978. Potential importance of benthic cysts of Gonyaulax tamarensis and G. excavata in initiating toxic dinoflagellate blooms. J. Phycol. 14, 224–234.

Aretxabaleta, A.L., McGillicuddy Jr, D.J., Smith, K.W., Lynch, D.R., 2008. Model simulations of the Bay of Fundy gyre: 1. Climatological results. J. Geophys. Res. 113 (C10027), http://dx.doi.org/10.1029/2007JC004480.

Aretxabaleta, A.L., McGillicuddy Jr, D.J., Smith, K.W., Manning, J.P., Lynch, D.R., 2009. Model simulations of the Bay of Fundy gyre: 2. Hindcasts for 2005-2007 reveal interannual variability in retentiveness. J. Geophys. Res. 114 (C09005), 10.1029/2008JC004948.

Bever, A.J., Harris, C.K., Sherwood, C.R., Signell, R.P., 2009. Deposition and flux of sediment from the Po River, Italy: An idealized and wintertime numerical modeling study. Mar. Geol. 260, 69–80.

Bigelow, H.B., 1927. Physical oceanography of the Gulf of Maine. Bull. U.S. Bur. Fish 49, 511–1027.

Blanton, B.O., 1993. User's Manual for 3-Dimensional Drogue Tracking on a Finite Element Grid with Linear Finite Elements. Technical report, UNC Marine Sciences, Chapel Hill, North Carolina, USA.

Brooks, D.A., 1985. Vernal circulation of the Gulf of Maine. J. Geophys. Res. 90 (C3), 4687–4705.

Brooks, D.A., 1994. A model study of the buoyancy-driven circulation in the Gulf of Maine. J. Phys. Oceanogr. 24, 2387–2412.

Brooks, D.A., Townsend, D.W., 1989. Variability of the coastal current and nutrient pathways in the eastern Gulf of Maine. J. Mar. Res. 47, 303–321.

Brown, W.S., Beardsley, R.C., 1978. Winter circulation in the western Gulf of Maine: Part 1. Cooling and water mass formation. J. Phys. Oceanogr. 8, 265–277.

Butman, B., Aretxabaleta, A.L., Dickhudt, P.J., Dalyander, P.S., Sherwood, C.R., Anderson, D.M., Keafer, B.A., Signell, R.P., 2014. Investigating the importance of sediment resuspension in *Alexandrium fundyense* cyst population dynamics in the Gulf of Maine. Deep-Sea Res. II 103, 79–95.

Chen, C., Liu, H., Beardsley, R.C., 2003. An unstructured grid, finite-volume, three-dimensional, primitive equations ocean model: Application to coastal ocean and estuaries. J. Atmos. Oceanic Technol. 20, 159–186.

Churchill, J.H., Pettigrew, N.R., Signell, R.P., 2005. Structure and variability of the Western Maine Coastal Current. Deep-Sea Res. II 52, 2392–2410.

Cowen, R.K., Gawarkiewicz, G., Pineda, J., Thorrold, S.R., Werner, F.E., 2007. Population connectivity in marine systems: an overview. Oceanography 20, 14–21.

Cowen, R.K., Paris, C.B., Srinivasan, A., 2006. Scaling of connectivity in marine populations. Science 311, 522–527.

Dietrich, W.E., 1982. Settling velocities of natural particles. Water Resour. Res. 18, 1615–1626.

Edwards, K.P., Hare, J., Werner, F.E., Seim, H.E., 2007. Using 2-dimensional dispersal kernels to identify the dominant influences on larval dispersal on continental shelves. Mar. Ecol. Prog. Ser. 352, 77–87.

Garrett, C.J.R., 1972. Tidal resonance in the Bay of Fundy and Gulf of Maine. Nature 238, 441–443.

Greenberg, D.A., 1983. Modeling the mean barotropic circulation in the Bay of Fundy and Gulf of Maine. J. Phys. Oceanogr. 13, 886–904.

Gust, G., Mueller, V., 1997. Hydrodynamics and Entrainment Functions of Currently Used Erosion Devices. In: Burt, N., Parker, R., Watts, J. (Eds.), Cohesive Sediments. John Wiley & Sons, London, pp. 149–174.

Hannah, C.G., Naimie, C.E., Loder, J.W., Werner, F.E., 1998. Upper-ocean transport mechanisms from the Gulf of Maine to Georges Bann with implications for Calanus supply. Cont. Shelf Res. 17 (15), 1887–1911.

Hill, P.S., Milligan, T.G., Geyer, W.R., 2000. Controls on effective settling velocity of suspended sediment in the Eel River flood plume. Cont. Shelf Res. 20, 2095–2111.

Holthuijsen, L.H., Booij, N., Ris, R.C., 1993. A spectral wave model for the coastal zone. In: Proceedings of the Second International Symposium on Ocean Wave Measurement and Analysis, New Orleans, Louisiana, July 25–28, 1993. New York, pp. 630–641.

Kirn, S.L., Townsend, D.W., Pettigrew, N.R., 2005. Suspended *Alexandrium* spp. hypnozygote cysts in the Gulf of Maine. Deep-Sea Res. 52, 2543–2559.

Lauzier, L.M., 1967. Bottom residual drift on the Continental Shelf area of the Canadian Atlantic coast. J. Fish. Res. Bd. Canada 24, 1845–1859.

Li, Y., He, R., Manning, J.P., 2014. Coastal connectivity in the Gulf of Maine in spring and summer of 2004–2009. Deep-Sea Res. II 103, 199–209.

Li, Y., He, R., McGillicuddy, D.J., 2014. Seasonal and interannual variability in Gulf of Maine hydrodynamics: 2002–2011. Deep-Sea Res. II 103, 210–222.

Lynch, D.R., Holboke, M.J., Naimie, C.E., 1997. The Maine Coastal Current: Spring climatological circulation. Cont. Shelf Res. 17, 605–634.

Manning, J.P., McGillicuddy, D.J., Pettigrew, N.R., Churchill, J.H., Incze, L., 2009. Drifter observations of the Gulf of Maine Coastal Current. Cont. Shelf Res. 29, 835–845.

Manning, J.P., Pelletier, E., 2009. Environmental Monitors on Lobster Traps: long-term temperature observations from New Englands bottom waters. J. Operational Oceanogr. 2-1, 25–33.

Martin, J.L., LeGresley, M.M., Hanke, A.R., 2014. Thirty years – *Alexandrium fundyense* cysts, bloom dynamics and shellfish toxicity in the Bay of Fundy, eastern Canada. Deep-Sea Res. II 103, 27–39.

McGillicuddy, D.J., Anderson, D.M., Lynch, D.R., Townsend, D.W., 2005. Mechanisms regulating large-scale seasonal fluctuations in *Alexandrium fundyense* populations in the Gulf of Maine: results from a physical-biological model. Deep-Sea Res. 52, 2698–2714.

Mitarai, S., Siegel, D.A., Watson, J.R., Dong, C., McWilliams, J.C., 2009. Quantifying connectivity in the coastal ocean with application to the Southern California Bight. J. Geophys. Res. 114 (C10026), http://dx.doi.org/10.1029/2008JC005166.

Mora, C., Sale, P.F., 2002. Are populations of coral reef fish open or closed? Trends Ecol Evol. 17, 422–428.

Pawlowicz, R., Beardsley, R.C., Lentz, S., 2002. Classical tidal harmonic analysis including error estimates in MATLAB using t_tide. Comput. Geosci. 28, 929–937.

Pettigrew, N.R., Churchill, J.M., Janzen, C.D., Mangum, L.J., Signell, R.P., Thomas, A.C., Townsend, D.W., Wallinga, J.P., Xue, H., 2005. The kinematic and hydrographic structure of the Gulf of Maine Coastal Current. Deep-Sea Res. II 52, 2369–2391.

Pettigrew, N.R., Fleming, R.J., Fikes, C.P., 2011. The history of the first decade of the observing system in the Gulf of Maine, and plans for the second decade. Mar. Technol. Soc. J. September 2011, 1–10.

Pettigrew, N.R., Townsend, D.W., Xue, H., Wallinga, J.P., Brickley, P.J., Hetland, R.D., 1998. Observations of the Eastern Maine Coastal Current and its offshore extentions in 1994. J. Geophys. Res. 103, 30623–30639.

Pilskaln, C.H., Hayashi, K., Keafer, B.A., Anderson, D.M., McGillicuddy, D.J., 2014. Benthic nepheloid layers in the Gulf of Maine and *Alexandrium* cyst inventories. Deep-Sea Res. II 103, 55–65.

Sanford, L.P., 2008. Modeling a dynamically varying mixed sediment bed with erosion, deposition, bioturbation, consolidation, and armoring. Comput. Geosci. 34, 1263–1283.

Sanford, L.P., Maa, J.P.Y., 2001. A unified erosion formulation for fine sediments. Mar. Geol. 179, 9–23.

Shull, D.H., Kremp, A., Mayer, L.M., 2014. Bioturbation, germination and deposition of *Alexandrium fundyense* cysts in the Gulf of Maine. Deep-Sea Res. II 103, 66–78.

Signell, R.P., 2010. Model data interoperability for the United States Integrated Ocean Observing System (IOOS). In: Spauldin, M. (Ed.), Proceedings of the Eleventh International Conference on Estuarine and Coastal Modeling. ASCE, pp. 221–238.

Vermersch, J.A., Beardsley, R.C., Brown, W.S., 1979. Winter circulation in the Western Gulf of Maine: Part 2. Current and pressure observations. Journal of Physical Oceanography 9, 768–784.

Warner, J.C., Sherwood, C.R., Signell, R.P., Harris, C., Arango, H., 2008. Development of a three-dimensional, regional, coupled wave, current, and sediment-transport model. Comput. Geosci. 34, 1284–1306.

Winterwerp, J.C., 2002. On the flocculation and settling velocity of estuarine mud. Cont. Shelf Res. 22, 1339–1360.

Xue, H., Chai, F., Pettigrew, N.R., 2000. A model study of the seasonal circulation of the Gulf of Maine. J. Phys. Oceanogr. 30, 1111–1135.

Xue, H., Incze, L., Wolff, N., Pettigrew, N.R., 2008. Connectivity of lobster populations in the coastal Gulf of Maine: Part I: Circulation and larval transport potential. Ecolog. Model. 210, 193–211.